3D Muscle Networks based on Vibrational Mechanomyography

C. Sebastian Mancero Castillo[1], **S. Farokh Atashzar**[2*] **and Ravi Vaidyanathan**[1,3*]

[1] Department of Mechanical Engineering, Imperial College London, London, UK
[2] Department of Mechanical and Aerospace Engineering, Department of Electrical and Computer Engineering, New York University, New York, USA
[3] UK Dementia Research Institute-CRT, Imperial College, London, UK
[*] Corresponding authors

E-mail: f.atashzar@nyu.edu and r.vaidyanathan@imperial.ac.uk

Keywords: Muscle Networks, Intermuscular Coherence, Mechanomyography.

Abstract. Objective: Muscle network modeling maps synergistic control during complex motor tasks. Intermuscular coherence (IMC) is key to isolate synchronization underlying coupling in such neuromuscular control. Model inputs, however, rely on electromyography (EMG), which can limit the depth of muscle and spatial information acquisition across muscle fibers.
Approach: We introduce three-dimensional muscle networks based on vibrational mechanomyography (vMMG) and IMC analysis to evaluate the functional co-modulation of muscles across frequency bands in concert with the longitudinal, lateral, and transverse directions of muscle fibers. vMMG is collected from twenty subjects using a bespoke armband of accelerometers while participants perform four hand gestures. IMC from four superficial muscles (flexor carpi radialis, brachioradialis, extensor digitorum communis, and flexor carpi ulnaris) is decomposed using matrix factorization into three frequency bands. We further evaluate the practical utility of the proposed technique by analyzing the network responses to various sensor-skin contact force levels, studying changes in quality, and discriminative power of vMMG.
Main Results: Results show distinct topological differences, with coherent coupling as high as 57% between specific muscle pairs, depending on the frequency band, gesture, and direction. No statistical decrease in signal strength was observed with higher contact force.
Significance: Results support the usability vMMG as a tool for muscle connectivity analyses and demonstrate the use of IMC as a new feature space for hand gesture classification. Comparison of spectrotemporal and muscle network properties between levels of force support the robustness of vMMG-based network models to variations in tissue compression. We argue three-dimensional models of vMMG-based muscle networks provide a new foundation for studying synergistic muscle activation, particularly in out-of-clinic scenarios where electrical recording is impractical.

1. Introduction

In the last decade, research on neural synchronization has been extended from neuron pair coupling [1] to the analysis of coherent neural organization for collective function [2, 3]. This has led to the study of the neural circuitry involved in the motor function as it facilitates the execution of complex motor activities [4] by coactivating collective groups of muscles to integrate sets of movements into a functional task [5, 6]. This coordinative activation of groups of muscles is driven by the central nervous system (CNS) [7] and is possible through synchronization and frequency encoding of neuronal activity governing motor control [8]. Muscle network analysis is an emerging tool (introduced in the last decade) to decode interactions between the CNS and the musculoskeletal system [9]. Drawing from graph theory and brain connectivity networks [10], this methodology describes the characteristics of complex neurophysiological structures of the musculoskeletal system during motor activities by mapping their topological representations and quantifying correlations in their properties [11]. Functional muscle networks are constructed by characterizing spectral synchronization of the neural motor control signals driving groups of muscles. This is achieved by extracting the intermuscular coherence (IMC) from surface electromyography (EMG) signals recorded from coordinative sets of muscles [9, 12].

Muscle connectivity is gaining traction as a tool to isolate key spectral characteristics of neural control to trace the actions of groups of muscles during complex repetitive motor control tasks [9, 13, 14]. For example, in [9], muscle network analysis was used to show distinct patterns of connectivity between muscles not only across the different postural tasks but also across constituent frequency bands. More recently, in [15] analysis of muscle networks was extended to different stages of the gait cycle, showing how network characteristics vary according to the gait cycle, how the neuromuscular system couples anatomical and functional linked muscles during locomotion, and how this information is encoded into different frequency band components. Studies in this arena have established the existence of task-specific changes with localized and widespread connectivity between muscles at multiple frequency bands depending on the task.

Despite growing interest, there remain relatively few studies regarding muscle connectivity network analysis [9, 13, 14, 16], all of which rely on EMG for muscle recording. EMG remains the gold standard for muscle measurement, however, it suffers from well-documented limitations imposed by (a) artifacts caused by skin-related impedance (e.g., sweat or scar tissue), (b) the need for specialized electronics, and (c) the pervasive electromagnetic noise which can hamper its use out-of-clinic [17, 18]. Mechanomyography (MMG) has been offered as an EMG alternative to surmount these limitations. MMG is a myographic modality that traces the mechanical response of the active motor units during a contraction as opposed to the electrical responses from the neural drive [19]. MMG spectral features have been found to contain valuable information regarding the physiological and contractile properties of skeletal muscles' motor units [19].

MMG use is poorly established and suffers from signal occlusion from vibrational artifacts, however, benefits such as ease of application, multiple uses for a single sensor, immunity to changes in skin impedance, and elimination of the need for skin preparation and conductive gel [20] offer significant potential for use in the field (i.e. out of laboratory/clinic). Muscle network analysis by the use of acoustic MMG (aMMG) was previously introduced by the authors in [21] for the evaluation of functional intermuscular connectivity alterations linked to upper-limb loss and differences in muscle network topologies derived from different hand gesture tasks. The results showed evidence that the spectral features of the aMMG signal can be used to construct muscle connectivity network modelS reflecting the common spectral patterns shared by upper-limb muscle groups when performing different motor tasks. Even though results support the suitability and information context of aMMG for muscle connectivity network analysis, aMMG is limited by the unidirectionality of signal acquisition without the ability to discriminate the information present along each of the different directions of propagation of MMG activity. The physiological and mechanical characteristics determining the direction of MMG propagation through muscle tissue are not yet fully understood. It has been suggested that oscillations generated during a muscular contraction propagate evenly in all directions from its origin (muscle central region [22] and active muscle fibers [23]). Such mechanical oscillations are attenuated in time as they propagate through soft tissues towards the skin

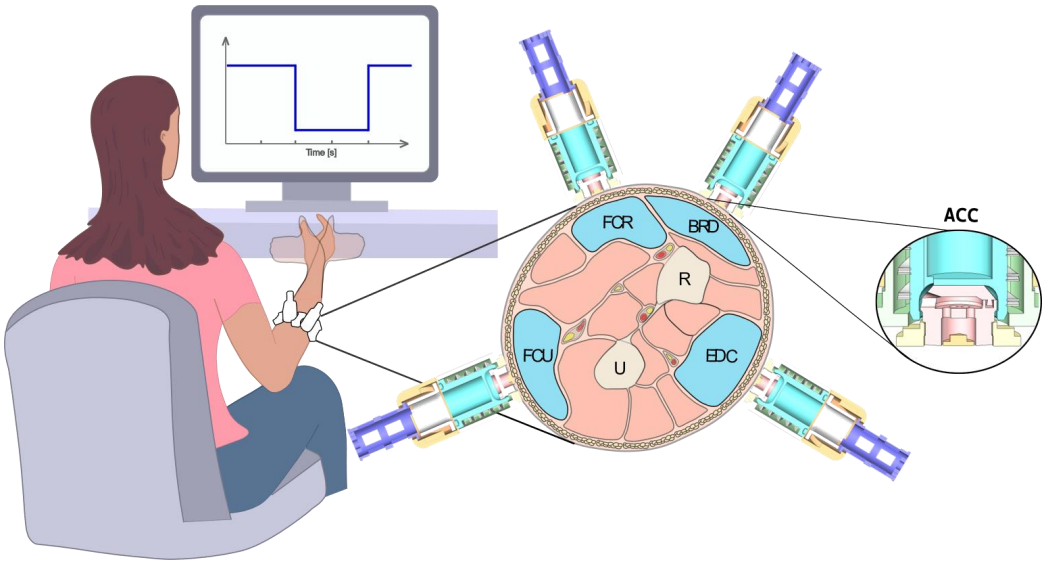

Figure 1. Experimental Layout. Participants were asked to perform four different hand gestures by following a square wave with a period of 10 s. The signal was displayed on a monitor to keep track of the duration of the contractions. Each contraction was sustained for a period of 5 s with the same time duration to rest between contractions. The cross-section view of the forearm is presented to illustrate the muscles of interest and sensor placement. Sensors were positioned over the flexor carpi radialis (FCR), brachioradialis (BRD), extensor digitorum communis (EDC), and flexor carpi ulnaris (FCU) muscles. A detailed cross-section view is shown on the right side to illustrate the accelerometer positioning in contact with the skin.

surface [24]. However, other studies suggest that the signal radiates mainly along the longitudinal and transverse directions with respect to the muscle fiber alignment [25, 26]. These findings suggest that the spectrotemporal properties of the MMG signal are subject to changes depending on the direction of propagation of the same.

The phenomenon of wave propagation of the MMG signal during the assessment of muscle activity needs to be further explored. For this purpose, vibrational MMG (vMMG) is a modality that gives the ability to measure the mechanical response of the muscle along the 3-axis (longitudinal, lateral, and transverse) with respect to the muscle fibers' alignment. In this work, we propose the analysis of the multi-directional space of the signal by introducing for the first time the concept of three-dimensional (3D) muscle networks based on vMMG for the analysis of the degree with which the mechanical responses caused by muscle activity propagate along the different directions of the muscle fiber alignment. This analysis allows for a more detailed evaluation of the muscle function from MMG activity as it detects the synergistic functionality of muscles during hand gesture tasks across the different directions of MMG propagation. We hypothesize that these three-dimensional muscle networks will show distinct topological characteristics not only between hand gestures at multiple frequency bands but also between the 3 directions of propagation, enabling a new perspective to study the intensity of MMG activity along the different directions of propagation. Furthermore, we hypothesize that the coherent activation of muscles, showing the common spectral patterns of muscle activity, is distinct enough between gestures and directions and can be further exploited to build discriminative models for hand gesture prediction.

Different myographic transducers have been applied in investigations to successfully capture the MMG signal. Typically, MMG modalities are affected by different factors, such as the length of the muscle being tested, external artifacts, cross-talk, and skin thickness [19]. Particularly, all MMG sensing modalities have been found to be influenced by the pressure with which the sensor is secured to the skin [27–29]. A recent study regarding the association of anthropometric parameters and the temporal features of vMMG [30] found that the signal remains invariant and robust to changes in arm diameter, muscle length, and skin-fold thickness, with also minimal crosstalk between arm and forearm muscles. However, there is a minimal investigation on the effect of changes in contact force between the sensor and the skin on not only the temporal but also the spectral features of the vMMG signal.

In [31], the authors demonstrated how different levels of contact force affect the temporal and spectral properties of the acoustic MMG signal, evident in changes in the signal-to-noise ratio and bandwidth, resulting in alterations in the discriminative power of the signal when discerning multiple hand gesture tasks. Results of the study indicate that increasing the normal force between the MMG sensor and the skin

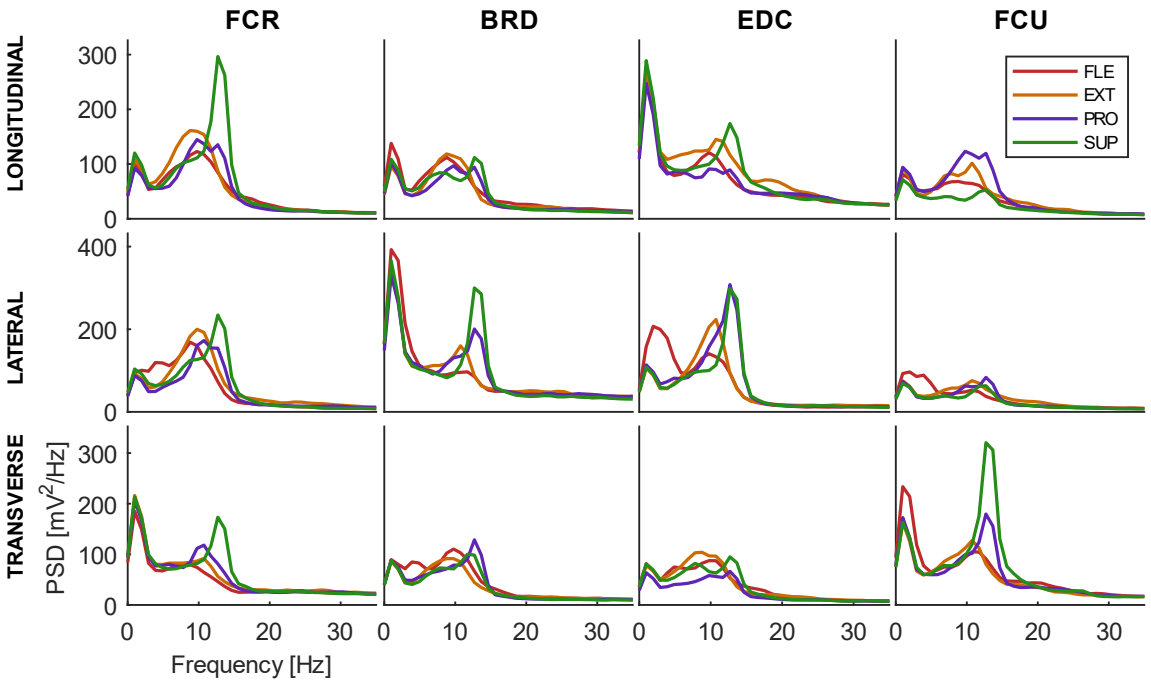

Figure 2. To obtain a unified spectral representation for each gesture, muscle, and direction of propagation, the power spectral densities obtained from all trials were averaged across both trials and participants. Power spectral densities shown for the different muscles (columns: FCR, BRD, EDC, and FCU) for all gestures (red: Flexion, yellow: Extension, purple: Pronation, and green: Supination) for each direction of propagation (rows: Longitudinal, Lateral, and Transverse).

causes subject-specific variations in the quality and discriminative power information for the classification of gestures. Previous studies on the effect of contact force on MMG activity indicate that higher levels of contact force result in an increase in the amplitude of the signal [27,28]. However, in the case of the vMMG, there is minimal investigation into this phenomenon. An initial study showed that progressively adding higher loads to the sensor (from 2 g to 50 g), thereof increasing the level of contact force, results in gradual signal distortion [29]. The lack of systematic investigation and understanding of this phenomenon on vMMG motivates the analysis of the quality and discriminative power of the signal under different levels of contact force.

To answer the above-mentioned research questions, four superficial muscles are considered to formulate the functional muscle networks during various hand gesture tasks. Intermuscular coherence is evaluated for all muscle pairs and used as the input space to generate the multi-directional muscle networks and to train classifier models for the prediction of hand gestures. In addition, we have previously shown how the spectrotemporal features of aMMG have sensitivity to the level of contact force attachment and how these variations can impact the usability of the signal [31]. In order to validate the robustness of vMMG to different levels of contact force in the context of muscle network analysis, we also perform the evaluation of the quality and discriminative content of vMMG under different levels of contact force.

The main objectives of this study are:

- Derivation of functional intermuscular connectivity between forearm muscle pairs at low, medium, and high-frequency bands by the use of a vMMG armband during the execution of four hand gesture tasks.
- Identification of multi-dimensional muscle networks, based on intermuscular coherence extracted from each axis of vMMG.
- Identification of distinctive characteristics in muscle network topologies based on the gesture performed, frequency band, and the direction of propagation.
- Implementation of classification models based on intermuscular coherence derived from vMMG to explore the gradient of discriminative information distributed along the different directions of propagation of the signal.
- Evaluation of the vMMG signal quality and discriminative power information to different levels of contact force.

2. Method

2.1. Participants

Twenty individuals (12 males, 8 females, mean age 25 ± 7 years old) participated in this study. All participants provided their written informed consent to take part in the study. All experiments were approved by the Imperial College Research Ethics Committee (ICREC reference: 15IC3068). This research was conducted in accordance with the principles embodied in the Declaration of Helsinki and in accordance with local statutory requirements.

2.2. Experimental Design

For this study, a four-channel accelerometer-based MMG armband was assembled following the design described in [31]. Data was collected using the custom-made vMMG armband comprised of four MC3635 3-axis accelerometer sensors configured with a resolution of ± 2 g. Accelerometers were positioned such that the axes were aligned with respect to the muscle fibers. The x-axis was aligned with the longitudinal direction, the y-axis was aligned with the lateral direction, and the z-axis was aligned with the transverse direction of the muscle fibers. Information was recorded while participants performed different hand gesture tasks. The experimental protocol followed the one described in [21]. For this study, gestures and target muscles were maintained. Namely wrist Flexion, Extension, Pronation, and Supination for gestures and flexor carpi radialis (FCR), brachioradialis (BRD), extensor digitorum communis (EDC), and flexor carpi ulnaris (FCU) for target muscles. Each participant was asked to follow a square wave presented on a monitor in front of them to keep track of the timing of the contractions (see 1 for an illustration of the experimental layout). Participants were asked to stay still for the duration of the experiment to minimize motion-induced artifacts. All participants performed a training trial which consisted of performing a series of sustained contractions of two randomly selected gestures. Each participant performed 7 repetitions of each gesture with intervals of 5 seconds of rest between each contraction. The experiment consisted of the same process as that of the training trial with gestures divided into two groups, each of two randomly ordered gestures. Intervals of 10 s of duration were applied at the beginning and the end of each of the two groups of recordings. The order of the gestures was randomized for each participant.

2.3. Data Processing

There have been various investigations dedicated to mitigating the presence of motion artifacts in the MMG signal [32–34]. The most common are Fourier-based techniques which include the use of Butterworth band-pass filters of different orders [32]. In this study, the raw signal of each MMG transducer was filtered using a fourth-order band-pass Butterworth filter in the range of 1 - 150 Hz, in accordance with previous literature regarding the active frequencies of MMG activity [19, 35]. The raw MMG signal of each channel was analyzed to extract only the steady-state phase of the contraction whilst discarding 1 second of information post-onset and pre-offset of the contraction. Three seconds of information were extracted for each contraction. MMG data was collected using a sampling frequency of 1 kHz.

Due to the time-varying properties of the MMG signal across multiple frequencies, it requires for its analysis the use of time-variant, frequency-selective techniques. A method commonly used is the Hilbert transform, an approach equivalent to Fourier and wavelet analysis [36] from which coupling measures such as coherence can be derived. In this study, the Hilbert transform was applied to obtain the analytic representation of the filtered MMG signal which is necessary for the estimation of the cross-spectrum and the power spectral density, both measures required in the generation of intermuscular coherence. These data processing steps were applied for information collected along each of the three directions of propagation of the signal.

2.4. Intermuscular Coherence

Intermuscular coherence (IMC) is a neurophysiological measure to evaluate the synchronization of neural activity between muscles during a motor task. IMC is confined between the values of 0 to 1. The higher the value of IMC, the more coupling of the muscles in the frequency domain. Intermuscular coherence was extracted between each muscle pair following the calculation described in [21] for the computation of modified magnitude squared coherence (MMSC). In order to consider the entire spectral space of the samples and to avoid the presence of spurious coherence caused by edge effects, each 3-second trial of data was zero-padded at both ends by a number of samples equal to half the samples needed to account for 1024 segments for the calculation of coherence. Coherence was then evaluated using Welch's method with segments of 1024 samples, a Nuttall window, and 50% of overlap. To prevent spurious coherence resulting from edge effects caused by the zero-padding process, each 3-second trial of information was first multiplied by a Tukey window using a cosine-tapered section of 0.05 [37]. Following these processing steps, IMC was calculated for each one of the seven trials. These IMC profiles were then

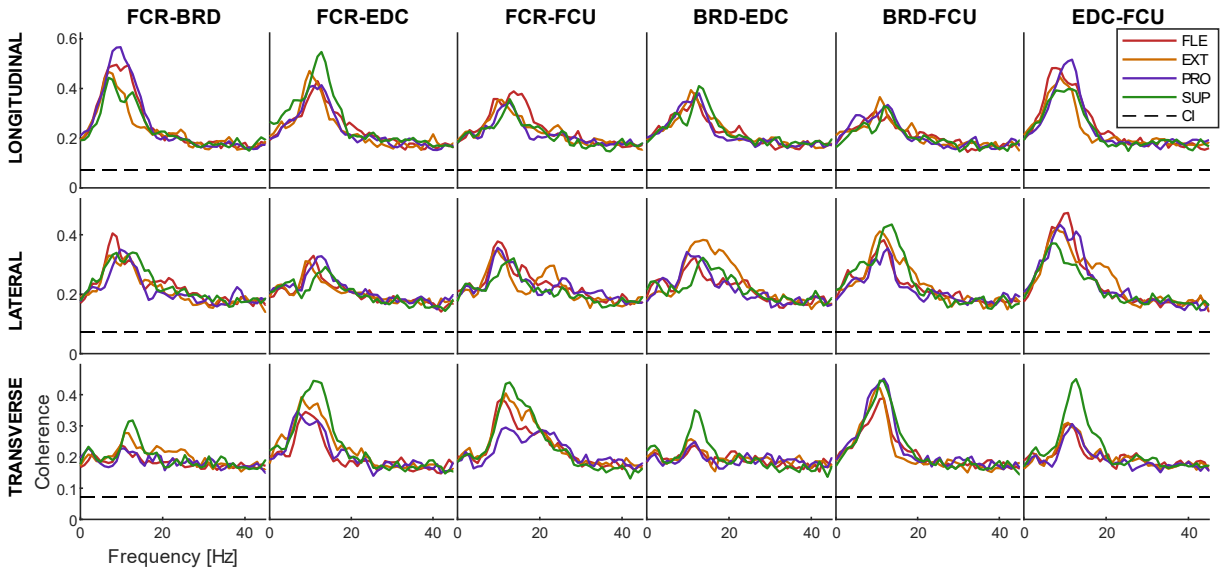

Figure 3. Intermuscular coherence between all muscle pairs (columns). Coherence is shown between all muscles for each gesture across every direction of propagation captured by the accelerometer (rows). Dashed line: confidence interval (CI)

averaged across trials. The resulting IMC profiles were subsequently averaged across participants for the purpose of obtaining a singular representation of muscle connectivity networks for each gesture. The IMC profiles from each participant were also maintained for further statistical evaluation of muscle network characteristics (see section 2.10). In this way, IMC was obtained for each participant and for the average of all participants for all muscle pairs, gestures, and directions, resulting in two matrices: one matrix of $(c_x m_x g_x d_x p)$, denoting c coherence values, m muscle pairs, g number of gestures, d number of directions, and p participants; and another matrix of only $(c_x m_x g_x d)$ for the average IMC of all participants.

2.5. Spectral Decomposition

Non-negative matrix factorization (NNMF) was used to decompose the generated IMC profiles into frequency band components to identify the common frequency space of the MMG signal at which the target muscles are co-modulated by the neural drive when performing different hand gestures and utilize these spectral characteristics to subsequently generate their corresponding muscle networks. Frequency band components were defined as 1-5 Hz for low-frequency information, 5–12 Hz for medium-frequency oscillations caused by tremor, and 12–40 Hz to capture high-frequency information produced by the inner muscle fibers oscillations, all of which constitute the MMG spectral space [38–40]. In this way, NNMF was applied to all coherence matrices $c_x m$ corresponding to each muscle pair, gesture, and direction. A multiplicative update rule was used to minimize the objective function and constraint the scope of each component to that of the frequency bands, as described in [21]. IMC of all muscle pairs was decomposed over the intervals specified above into non-negative factors using an alternating least squares algorithm, thus resulting in two non-negative matrices reflecting the spectral signatures (basis vectors) and the corresponding coupling strengths between all muscle pairs for each gesture and each direction.

2.6. Muscle Networks

Basis vectors along with the coupling strengths generated for each of the frequency band components were used to extract task- and frequency-specific matrices for each gesture and each direction. The resulting adjacency matrices were then used to generate the undirected weighted functional connectivity networks. Muscle networks are constructed so that each target muscle represents a node in the network and the edges of the network are defined by the connections between the nodes, denoted by the basis vectors obtained from the NNMF process. Figure 4 shows the muscle networks generated for the average IMC of all participants for each gesture (columns) and frequency component (rows) for each direction.

The clustering coefficient (CC) of a network is a measure that quantifies the degree of connectivity between the nodes. It provides insights into the local structure of the network by assessing how closely connected the immediate neighbors of a node are to each other. The CC is averaged across nodes

to obtain a global measure of the network. In an undirected weighted network, global efficiency (GE) is a measure to quantify the efficiency of information transfer across the entire network. It provides insights into how well a network facilitates communication and integration between its nodes, with higher values of GE indicating a more functionally integrated network. The computation of CC and GE was computed for all connectivity networks generated from each participant along all directions, frequency components, and gestures. The CC values were averaged across nodes to obtain a global measure of each network [11].

2.7. Feature Extraction

For the purpose of training a multi-class classification model based on IMC, information from each trial was segmented into windows of 0.97 ms (1024 samples) with 50% of overlap. IMC was calculated following the same process mentioned above for each one of the generated segments. In order to improve computational speed, the feature space was reduced to discard IMC information at frequencies higher than 256 Hz as they have a negligible effect on classification performance. IMC data from all muscle pairs for the entire frequency domain were concatenated to generate the feature space. The feature space was subsequently segmented using a hold-out validation method consisting of 80% of the data used for training and 20% used for testing. A multi-class support vector machine (SVM) model was used as it is a relatively simple and computationally effective machine-learning technique that has been successfully used in biosignal classification [41, 42].

2.8. Contact Force

Making use of the sensor design described in [31] adapted for vMMG sensors, the experimental protocol described above was also performed using a second level of contact force. To ensure consistency, during the first part of the experiment described above the first level of contact force was determined by matching the length of the armband with the arm diameter of each participant. The second level of contact force consisted of protruding each sensor 3 mm onto the skin while maintaining the same length of the armband and without removing it, effectively increasing the level of contact force between the sensor and the skin and ensuring the same sensor location.

2.9. Spectrotemporal Features variations

Temporal and spectral features of the MMG signal have been shown to contain essential information regarding neuromuscular control of muscles, providing important insights into the strategies of motor unit recruitment and firing rate [43, 44]. Gaining a better understating of how changes in contact force alter the features of vMMG could improve the usability of the signal for the analysis of the neuromuscular function of the muscles. In order to evaluate the spectrotemporal changes between the levels of contact force for the MMG response, three temporal metrics and three spectral metrics were extracted for each channel/muscle, gesture, and level of force in all directions.

Temporal domain features include:

- Root Mean Square (RMS): RMS is a widely used feature in MMG activity commonly employed for the analysis of fatigue, force production, toque [45], and has also been used for hand gesture classification [46].
- Log Detector (LOG): LOG is a feature commonly used in EMG to obtain an estimate of muscle contraction [47] and it has recently been used in MMG for the estimation of muscle strength [48].
- Waveform Length (WL): WL is defined as the cumulative length of the signal over time segments and it is a measure of the complexity of the signal.

Frequency domain features include:

- Mean Frequency (MNF): MNF is a spectral feature calculated as the summation of the product between the frequency and the power present at that frequency divided by the total power spectrum.
- Peak Frequency (PKF): PKF is known as the frequency at which the maximum power occurs.
- Mean Power (MNP): MNP is defined as the average power of the spectral response of the MMG signal. Similar to RMS, this feature has been used in the literature for the analysis of torque [44].

All the extracted features were averaged across participants. To show variations of the spectrotemporal features between the first and second level of contact force, the percentage change for each feature was computed as follows:

$$\%feature_{change} = \frac{feature_{FL2} - feature_{FL1}}{feature_{FL1}} \cdot 100 \quad (1)$$

with, FL referring to force levels.

2.10. Statistical Analysis

In this study, four statistical comparisons were performed. The first consisted of comparing the temporal and spectral features between levels of force for each muscle, gesture, and direction to

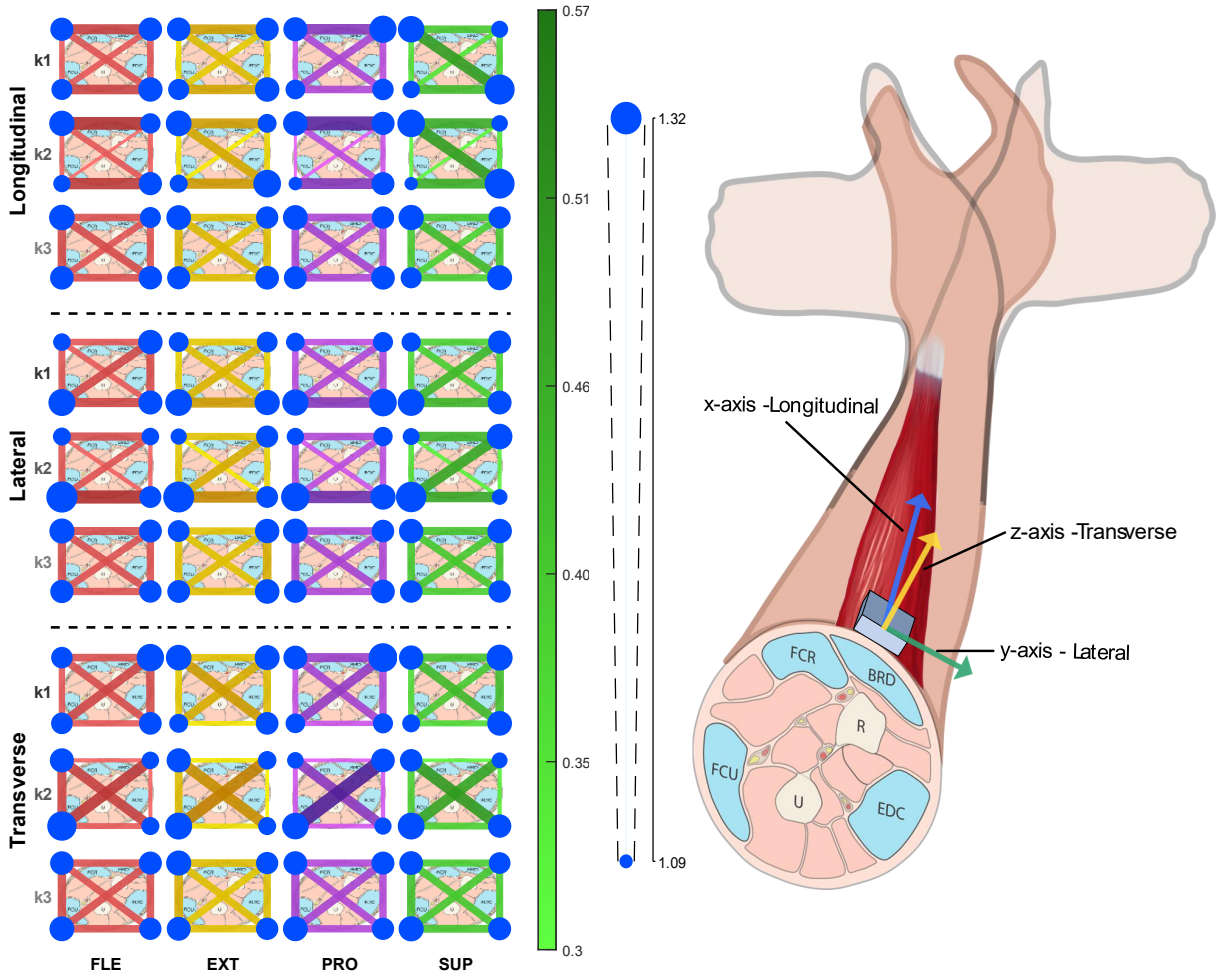

Figure 4. Intermuscular coherence between muscle pairs was decomposed into three frequency bands using non-negative matrix factorization. The three frequency components were defined as: k1: 1-5 Hz, k2: 5-12 Hz, and k3: 12-40 Hz. Left-side, muscle connectivity networks were extracted for each gesture (columns) at each of the frequency components (rows) for all axes (groups of rows). Functional networks were generated using the common spectral patterns and the corresponding weightings across frequency bands. Weightings were used to define the strength of the connections (edges) between muscles (nodes). Connectivity strength is illustrated by the gradient of color defined by the color bar and the thickness of the connection. Node strength is illustrated by the size of the node and it is defined by the weightings of the edges connected to the muscle. Right-side, cross-section view of the forearm for illustration of the positioning of a single accelerometer sensor over a target muscle. Each accelerometer was aligned such the x-axis was co-lineal with the longitudinal direction of the muscle fiber, the y-axis was co-lineal with the lateral direction, and the z-axis was aligned with the normal direction.

evaluate statistically significant changes in the quality of the signal when different levels of contact forces are applied. The second statistical comparison consisted of comparing the clustering coefficient and global efficiency of the muscle networks between the levels of force to statistically evaluate changes in the muscle network characteristics at different levels of contact force. The third statistical comparison consisted of comparing the performance accuracy of the classification models between levels of force for each classification model. The fourth statistic was performed to compare the performance accuracy of classification models between the single-direction vs multi-direction trained models.

Data from the second statistical comparison did not pass the normality test. The statistical comparison for this dataset was performed using Wilcoxon signed rank test. Data from the rest of the statistical comparison passed the Shapiro–Wilk normality test. These statistical comparisons were performed using a t-test to determine significance. Statistical significance was considered for values of $p\text{-}values < 0.05$. Bonferroni-adjusted significance was computed to minimize type-I errors. The adjusted significance level for the first statistical comparison was $adjusted\text{-}p\text{-}value = 0.0031$. The adjusted significance level for the second statistical comparison was $adjusted\text{-}p\text{-}value = 0.0041$. The adjusted significance level for the third statistical

comparison was *adjusted-p-value* = 0.0125. The adjusted significance level for the fourth statistical comparison was *adjusted-p-value* = 0.0166.

3. Results & Discussion

In this study, we analyzed the intermuscular coherence between muscle pairs from four superficial muscles in the forearm for the generation of task-specific muscle networks and the evaluation of a classification model for the detection of hand gestures. Following the signal processing steps and after obtaining the analytic representation of the signal, the power spectral densities (PSDs) were extracted for each of the trials for all gestures. PSDs were averaged across trials and subsequently averaged across participants to obtain a singular power spectral response for each muscle when performing the different gestures along each direction of propagation. Figure 2 shows the PSDs for all gestures for each muscle (columns) and each direction/axis (rows). PSDs of all directions showed power information at frequencies no higher than 40 Hz, with minimal power found at higher frequencies. Interestingly, the PSDs across directions show similar profiles with distinct power information depending on the gesture, muscle, and direction.

3.1. Muscle-Pairs Coherence

Intermuscular coherence was calculated for each muscle pair for all gestures, participants, and directions. Figure 3 shows the IMC activity for all muscle pairs (columns) for each direction/axis (rows). The confidence interval is calculated following the method described in [49] for overlapped segments. IMC values ranged from values of 0.3 to 0.57. Previous studies based on EMG have found coupling strengths between muscle pairs no higher than 0.2 [9], [50] for lower- and upper-limb, respectively. IMC based on MMG is a new area of study initially proposed by the authors. In [21] we found coupling strengths as high as 0.55 by the use of acoustic MMG. In line with these previous findings, results here show similar values of coupling strengths for vMMG.

IMC shows functional activation at multiple frequencies with distinct profiles across muscle pairs and similar spectral common responses across gestures with different scaling factors. Coherent activation across muscles is observed at multiple frequencies below 40 Hz. IMC results show high levels of connectivity for FCR-BDR, FCR-EDC, and EDC-FCU muscle pairs along the longitudinal direction, widespread common spectral activity across the lateral direction, and high connectivity for FCR-EDC, FCR-FCU, and BDR-FCU muscle pairs for the transverse direction. For the transverse direction, different from the other two directions, low levels of IMC were found for FCR-BDR, BDR-EDC, and EDC-FCU muscle pairs. IMC for the different hand gestures shows common frequency information across directions with distinct profiles for specific muscle pairs. Flexion shows the highest IMC for FCR-BDR and EDC-FCU muscle pairs along the longitudinal and lateral directions, with low IMC along the transverse direction. Extension shows a distinct higher activity of IMC in the lateral direction across muscle pairs BDR-EDC, BDR-FCU, and EDC-FCU. Higher coherent activity compared to Flexion was found along the transverse direction for Extension. Pronation shows the highest IMC in the longitudinal direction for the FCR-BDR muscle pair. Supination shows distinctively higher levels of IMC compared to the other gestures across all muscle pairs in the transverse direction. The highest peak of IMC for Supination was found for FCR-EDC.

3.2. Muscle Networks

Intermuscular coherence found across the frequency spectra were decomposed into frequency ranges according to the spectral bands of interest (i.e., 1-5, 5-12, 12-40 Hz). Basis vectors and coupling strengths resulting from the spectral decomposition were used to generate muscle connectivity networks for each gesture at each frequency component for every direction. Figure 4 shows the functional connectivity networks for all gestures (columns) at each frequency band component (rows) for the three directions of vMMG (groups of rows). Symmetric networks are illustrated for better identification of connectivity distinctions between muscle pairs.

3.2.1. Longitudinal networks

The first component, capturing IMC at frequencies from 1-5 Hz, yields distinct connectivity topologies between gestures. Flexion shows strong connections between medial forearm muscles (FCR-BRD) and lateral muscles (FCU-EDC). Extension shows a similar topology with higher connectivity compared to flexion between FCR-EDC muscles. Pronation shows strong connectivity between FCR-BRD. Supination shows a strong connection between FCR-EDC muscles. The second frequency component yielded similar topologies to those of the first frequency component with stronger and more evident distinctions in connections between muscle pairs. In this component. Flexion shows stronger connectivity between FCR-BRD. High connectivity is also found between FCU-EDC. Similarly, Extension shows strong connectivity between FCR-BRD and FCU-EDC, with a stronger connection between FCR-EDC muscles. Pronation shows a similar topology to that of Flexion, with

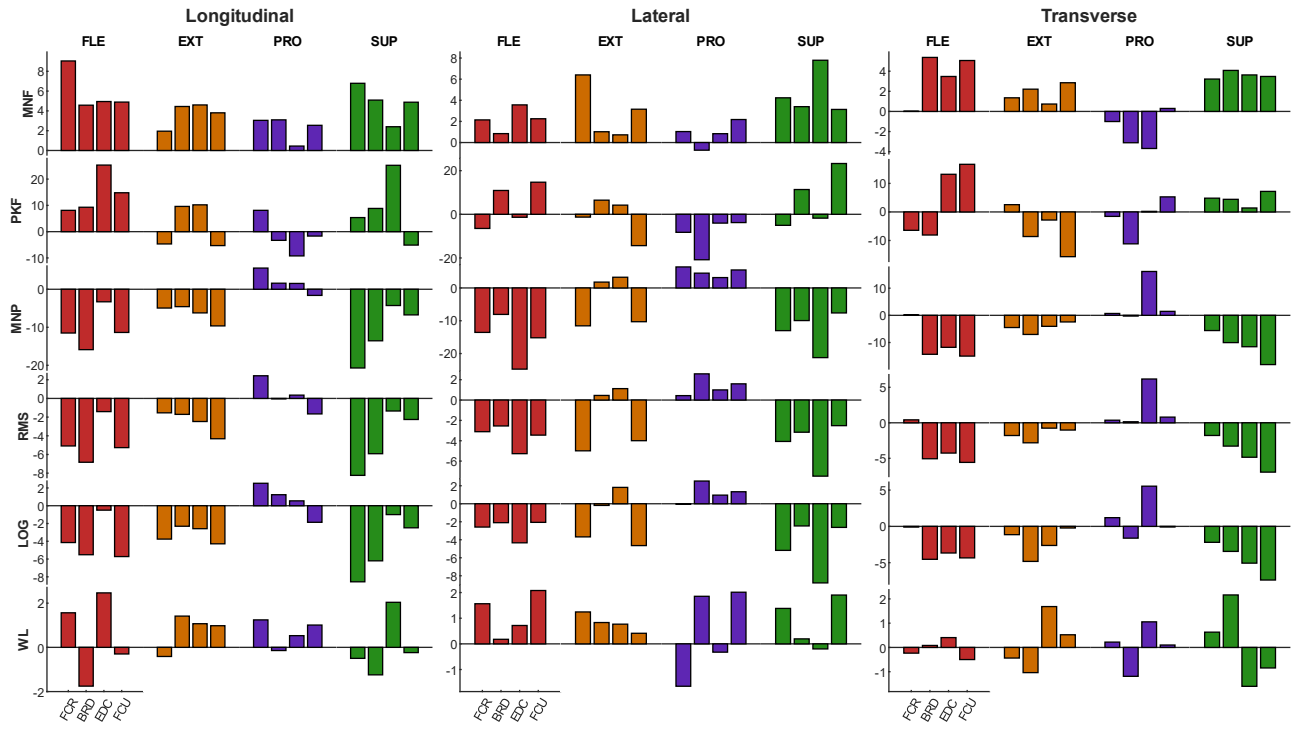

Figure 5. To analyze the effect of contact force in the time and frequency domain of the MMG signal, three temporal (MNF, PKF, MNP) and three spectral (RMS, LOG, WL) features of the MMG activity were extracted for all muscles, gestures, directions and averaged across trials and participants. The percentage variations of the features from the first level of contact force to the second level of contact force are shown for each spectrotemporal feature (rows) for every muscle (bars), gesture (color-coded groups of bars), and for all directions (columns).

strong connections between FCR-BRD and FCU-EDC. Supination presents a similar topology to Extension, with strong connections between FCR-BRD, FCU-EDC, and even stronger connectivity for FCR-EDC. The lowest levels of connectivity across gestures and components were found between FCU-BRD. The third frequency component shows widespread medium levels of connectivity across muscles for all gestures. This component shows stronger connectivity for all gestures between anterior and posterior muscle pair connections compared to the first two components. Figure 4 indicates a transition from localized connectivity between muscle pairs at low frequencies (i.e., 1-5 Hz) to stronger localized connections at medium frequencies and widespread connectivity at high frequencies.

3.2.2. Lateral networks

The first component shows medium-to-high connectivity between the FCU-BRD-EDC triplet for Flexion. High connectivity between FCU-EDC and medium connectivity for FCU-BRD and FCR-BRD was found for Extension. Pronation shows strong connectivity for the FCU-EDC muscle pair. Supination shows strong connectivity for FCU-EDC with medium to high levels of connectivity for FCU-BRD and FCR-EDC. In general, the muscle pair FCU-EDC shows strong levels of connectivity across gestures, with FCU-BRD showing a similar characteristic with medium levels of connectivity. For the second component, a phenomenon similar to the longitudinal direction was found, where the connectivity between muscles shows a higher level of connectivity compared to those of the first component. Flexion shows strong connectivity between FCR-BRD muscles. Extension shows a similar topology to Flexion with medium levels of connectivity between FCU-BRD. Pronation shows high connectivity between FCU-EDC with low levels of connectivity between the rest of the muscles. Supination shows strong connectivity between FCR-BRD, FCU-BRD, and FCU-EDC. Interestingly, the second component for the lateral direction shows characteristic low connectivity between FCU-BRD muscles across all gestures and medium to low connectivity between anterior and posterior muscle pair connections. The third component shows medium levels of connectivity across muscles and gestures. This component shows an increase in connectivity for FCU-BRD across all gestures compared to the previous component and a similar behavior for FCU-FCR and BRD-EDC.

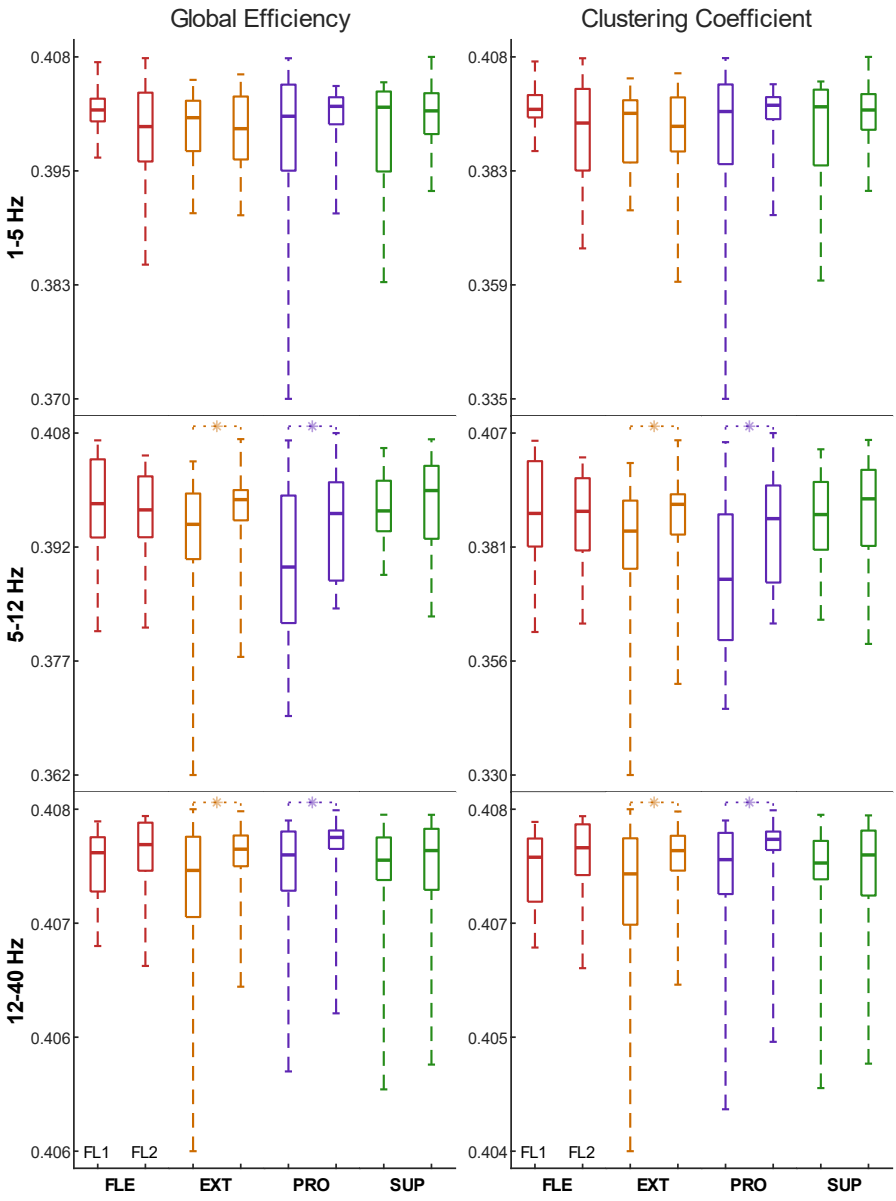

Figure 6. Boxplots for the Transverse direction of global efficiency (left) and clustering coefficient (right) of muscle networks generated from all participants for force level (FL) 1 and 2 for all gestures within each of the frequency band components. Significance is shown with $*$ for p-value<0.05. The statistical comparison showed no significance at Bonferroni adjusted-p-value<0.0041

3.2.3. Transverse networks

The first component for the transverse direction shows widespread connectivity for most muscle pairs across gestures with distinctive low connectivity between FCR-FCU and FCU-EDC. Medium to high levels of connectivity are found between FCU-BRD and FCR-EDC and medium to low levels of connectivity are found between FCU-EDC and FCR-FCU across gestures. The second component shows topologies similar to the first component with more evident differences in connectivity strength between muscle pairs. Flexion shows strong connectivity between FCU-BRD and FCR-EDC and heterogeneous connectivity between the rest of the muscle pairs. Extension shows distinctively strong connectivity between the same muscles (FCU-BRD and FCR-EDC). Pronation shows the highest connectivity across gestures, components, and directions between FCU-BRD. Medium to high connectivity is found between FCR-EDC and a characteristic low connectivity strength is found between the peripheral connections. Supination shows a similar topology to those of Flexion and Extension. For this component, characteristic low connectivity between FCR-BRD and BRD-EDC

is found across gestures. In the third component, similar topologies to those of the first two directions are found with widespread connectivity between all muscle pairs across gestures. Muscle connectivity strength increased for muscle pairs FCR-BRD and BRD-EDC compared to the second component.

3.2.4. Functional Muscle Networks

The longitudinal direction shows strong connectivity between FCR-BRD and FCU-EDC across gestures and low connectivity between FCU-BRD. The lateral direction shows high connectivity between FCU-EDC and low connectivity between the diagonal connection FCR-EDC across gestures. The transverse direction shows strong connectivity between the diagonal muscle connections FCU-BRD and FCR-EDC.

Regarding the role of each muscle during the gestures, both flexor muscles and the extensor digitorum communis play a role in wrist Flexion and Extension, therefore it is to expect a high functional activation of the FCR-FCU-EDC muscles. FCU shows high connectivity with the EDC muscle across directions. FCR-EDC shows high connectivity along the transverse direction only. The BRD muscle shows high connectivity with the FCR along the longitudinal direction. Similarly, high connectivity was found for FCU and EDC muscles for Extension along the longitudinal and lateral dimensions, and a strong connection between FCR-EDC muscles for the lateral and transverse direction. The brachioradialis muscle is in its majority responsible for gestures Pronation and Supination; therefore, a higher level of connectivity is expected for vertices connected to the BRD muscle during those gestures. High connectivity between FCU-BRD is found for the lateral direction and more evidently for the transverse direction. Similar topologies were found between Extension and Supination across directions for the second frequency component. The highest levels of connectivity were found along the longitudinal and transverse directions, suggesting a higher propagation of the MMG signal in these directions in line with the directional propagation of mechanomyography activity longitudinally and normal with respect to the muscle fibers according to previous findings [25].

The functional strengthening of muscle connectivity from the first to the second frequency component seen across directions suggests overlapping spectral responses between low-frequency oscillations caused by movement and tremor, respectively, with tremor accounting for the majority of the common spectral power between muscles. This common characteristic for the first two components across directions suggests a multi-directional propagation of the mechanomyography activity along the longitudinal, lateral, and transverse directions. The distinct differences in the topology of the networks between directions suggest unique spectral information of the mechanomyography contained along each of the three directions of muscle fiber alignment. The MMG signal originates from a contraction as the length of the muscle fibers shortens and the fiber diameter increases [51]. During a contraction, as the muscle fibers shorten and the muscle is being pulled towards its origin, the transverse diameter of the muscle changes in shape (increases) at the level of the muscle belly [52]. The lateral oscillations of the muscles as well as the dimensional changes of the muscle fibers produce pressure waves that propagate through muscle tissue and are detectable on the surface of the skin. This characteristic of the MMG signal could explain the differences in topologies found across directions. In [53], their analysis showed that during isometric voluntary contractions, the muscle remains in a state of vibration in which all locations along the longitudinal axis of the muscle vibrate in phase, and sensors located perpendicular to the longitudinal axis vibrate with opposite phases, suggesting that the MMG signal is a reflection of the muscle as a global resonant structure to the local fluctuations of pressure which propagate along all the different directions of muscle fiber alignment. The similar topological signatures found for the different directions along the third frequency component suggest common oscillatory activity across directions at high frequencies, in line with previous findings of coherent analysis between directions of MMG propagation [53].

For future studies, we expect that the functional muscular connectivity analysis by the use of MMG could provide a better tool for the study of the underlying neuromuscular parameters responsible for muscle contraction, making it a reliable tool for muscle function assessment [54]. The MMG signal properties have proved to be fundamental when assessing muscle function and performance in the medical field [55]. Numerous investigations have shown how properties derived from vibration can be used to evaluate muscle activity and muscular performance [19]. MMG has been used in clinical applications to detect and monitor muscular pain [41], diagnose muscle hypertrophy and atrophy [56], and for the examination of neuromuscular disorders [57]. A better understanding of the composition and characteristics of the MMG signal could strengthen the usability of the myographic signal. Thus, the analysis of the multi-directional space of the MMG signal is essential not only for a better understanding of the physiological aspects responsible for muscle contraction but also for making MMG a more reliable tool for muscle function assessment while broadening the potential use of the signal into new fields of study.

3.2.5. Muscle Network Properties

Figure 6 shows results for the clustering coefficient and global efficiency for all frequency components (rows), gestures (color-coded), and levels of force (FL1, FL2) for the Transverse direction.

For both metrics, GE and CC, the possible values can range from 0 to 1 depending on the efficiency in facilitating information exchange between nodes and the degree of local clustering among nodes, respectively. For the first frequency component, the values of the clustering coefficient varied minimally between levels of force and between gestures, with a similar behavior found for global efficiency. The second component shows more variations compared to the first component, with Extension and Pronation showing an increase ($p < 0.05$) between the first and second levels of contact force for GE and CC. For the third component, results for CC and GE yielded values between 0.407 and 0.408 across gestures for both levels of force. Similar to the second frequency component, Extension and Pronation showed an evident increase in GE and CC between the first and second levels of contact force. All these differences for the second and third frequency component were found to be not significant at the adjusted p-value: 0.0041. The results of GE showed similar values to those of CC for all gestures and frequency components. The highest value of GE and CC was 0.408. The smallest value of GE and CC was found at the first level of contact force for Extension, yielding 0.362 and 0.330, respectively. A clustering coefficient of 0.330 and no higher than 0.408 means that, on average, nodes in the network have relatively strong local connections with their neighbors. A global efficiency between 0.362 and 0.408 suggests that, on average, it is relatively efficient to transmit information between nodes in the networks. However, having similar levels of GE and CC in the network suggests a balance between local clustering and global information exchange within the networks, indicating the formation of network structures with a balance between well-defined local clusters, while still maintaining a relatively efficient exchange of information between distant parts of the network. In the context of muscle networks, this means that during a motor action (e.g., hand gesture) muscles that are actively involved in that particular action tend to form a cluster (synergy), but the network of muscles allows for the information or influence of the cluster to propagate through the different connections to reach muscles which are not directly involved in that particular motor activity. This previously mentioned analysis was also performed for the longitudinal and lateral directions. Results showed minimal variations between levels of force for GE and CC with no significant differences found between levels of force.

It is important to mention that the size of the networks (i.e., 4 nodes/muscles) could have an influence on the similarity between values of GE and CC since small networks provide fewer possible configurations of both clusters and paths of information interchange which can lead to similar values of these measures. As a future direction of this study, we intend to include a higher number of muscles during not only static but also dynamic actions.

3.3. Spectrotemporal Features variations

Figure 5 shows the percentage change of each spectrotemporal feature from force level one to force level two for all muscles, gestures, and directions.

Results from the longitudinal direction show an increase in the MNF values across muscles and gestures, suggesting an increase in the power across frequencies. A similar characteristic is also found for the PKF for Flexion and Supination, with a common decrease for the FCU muscle for most gestures except for Flexion. Results from MNP show a general decrease in values across gestures, with the exception of Pronation. RMS and LOG showed a similar characteristic with decreases across gestures with the exception of Pronation, which showed a minimal increase in both features. The decrease in RMS indicates a lower average amplitude of the signal for the second level of force, in line with results in MNP. The decrease in LOG, implying a decrease in muscle contraction could be explained as a result of limited mobility of the muscles at higher levels of contact force. WL showed heterogeneous variations across muscles and gestures between levels of contact force.

Results from the lateral direction show a less pronounced increase in the MNF compared to the longitudinal direction, showing in general small increases across gestures. Heterogeneous variations were found for the PKF across gestures with small variations of this feature between contact force levels. Results from the MNP show a decrease across muscles for Flexion and Supination, small increases across muscles for Pronation, and small variations for Extension. These results, similar to the longitudinal direction, showing a decrease in the MNP and an increase in MNF indicate lower power information is found in the second level of contact force with a shift of the active frequencies in the first level towards higher frequencies at the second level of contact force, resulting also in increases for the PKF. Pronation showed the opposite characteristic for both directions, showing an increase for both MNP and MNF with a decrease in PKF. These results suggest a shift of the power information of the active frequencies in the first level of force towards lower frequencies at the second level of contact force, hence producing lower

PKF at the second level of force. RMS and LOG show a decrease across gestures except for Pronation which, as expected from the spectral features, shows the opposite characteristic compared to the rest of the gestures. WL shows an increase across muscles for Flexion, Extension, and Supination, and for anterior muscles for Pronation. A decrease in WL was found for posterior muscles during Pronation.

Results from the transverse direction show increase in MNF for Flexion, Extension, and Supination, and a decrease in Pronation. Heterogeneous variations were found across muscles and gestures for the PKF with Supination showing an increase across all muscles. MNP presents a decrease in the average power information for Flexion, Extension, and Supination. Minimal changes were found for Supination across muscles with a characteristic increase for EDC muscle. Similar characteristic variations across muscles and gestures were found for RMS and LOG. WL shows the lowest variations across directions and heterogeneous variations across muscles depending on the gesture. Results of WL across directions show that the characteristic complexity of the signal for each muscle and gesture is detected in all directions of vMMG. The lowest variations across temporal and spectral features were found for Pronation across all directions.

3.4. Gesture Classification

Figure 7 shows the confusion matrices and the distribution of the accuracies for the gesture classification models trained using IMC from individual directions and from the combination of all directions. For the longitudinal direction, Extension, and Pronation were classified correctly more generally than Flexion and Supination. Extension shows the highest rate of classification across gestures for both levels of contact force. Supination shows the lowest classification rate across gestures for both contact force levels, with the majority of miss-classifications being identified as Pronation for the first level of contact force and as Extension for the second level of contact force. In the lateral direction, Flexion showed the highest rate of classification for the first level of force, with Pronation and Supination showing the lowest rates. In the second level of force, Pronation yielded the highest classification rate and Supination showed the lowest. In general, classification rates decreased in performance between the first and second levels of contact force with the exception of Pronation, which showed an increase in the classification rate. For the transverse direction, the highest classification rate was found for Pronation and the lowest accuracy was found for Flexion in the first level of contact force, with the majority of miss-classifications identified as Pronation. The second level of contact force showed in general a decrease in classification performance compared to the first level of force and similar levels of classification accuracies across gestures. In the case of the multi-directional trained model, the highest classification rate was found for Flexion for the first level of contact force and Extension for the second level of contact force. The lowest classification performance was found for Supination for both force levels.

The lowest accuracies were found for the models trained using longitudinal direction IMC features. Models trained using IMC features along the lateral direction yielded the highest performance between directions. The model performance for the second level of force shows higher variance compared to the first level of force across directions. However, the opposite results are found for the model trained using features from all directions, showing less variance in accuracy distribution for both levels of force. The classification accuracy of the models shows similar performance between the two levels of force across directions. The average accuracy of classification for the first level of force in the longitudinal direction is 57.50 %, which increased to 60.36% for the second level of force. The accuracy of classification for the lateral direction and transverse direction decreased between the first and the second level of force. Classification for the lateral direction yielded 67.87% and 65.36% for the first and second levels of force, respectively. Classification accuracy for the transverse direction shows a decrease from 65.18% to 61.25%. The average classification accuracy of the multi-directional trained model showed a substantial increase in accuracy with similar performances between levels of force, yielding 84.11% and 83.75% for the first and second levels of contact force, respectively.

There have only been a handful of investigations in which solely vMMG has been used for the classification of motor tasks. Investigations commonly employ a combination of MMG features along with other modalities such as IMU [58] and EMG [59] in order to achieve higher rates of motor intention detection. Studies in which advanced machine learning techniques have been used with vMMG as a standalone tool for gesture classification have found accuracies of 87% [60] and 91% [61]. However, these studies are limited to a small number of gestures and isometric activities. The findings showcased in this study are anticipated to serve as a catalyst for adopting the novel feature space based on IMC and emphasize the significance of considering the information content across all the directions of MMG propagation to encourage the development of more robust and accurate models for motor intention detection for a larger number of muscles during statics as well as dynamic tasks.

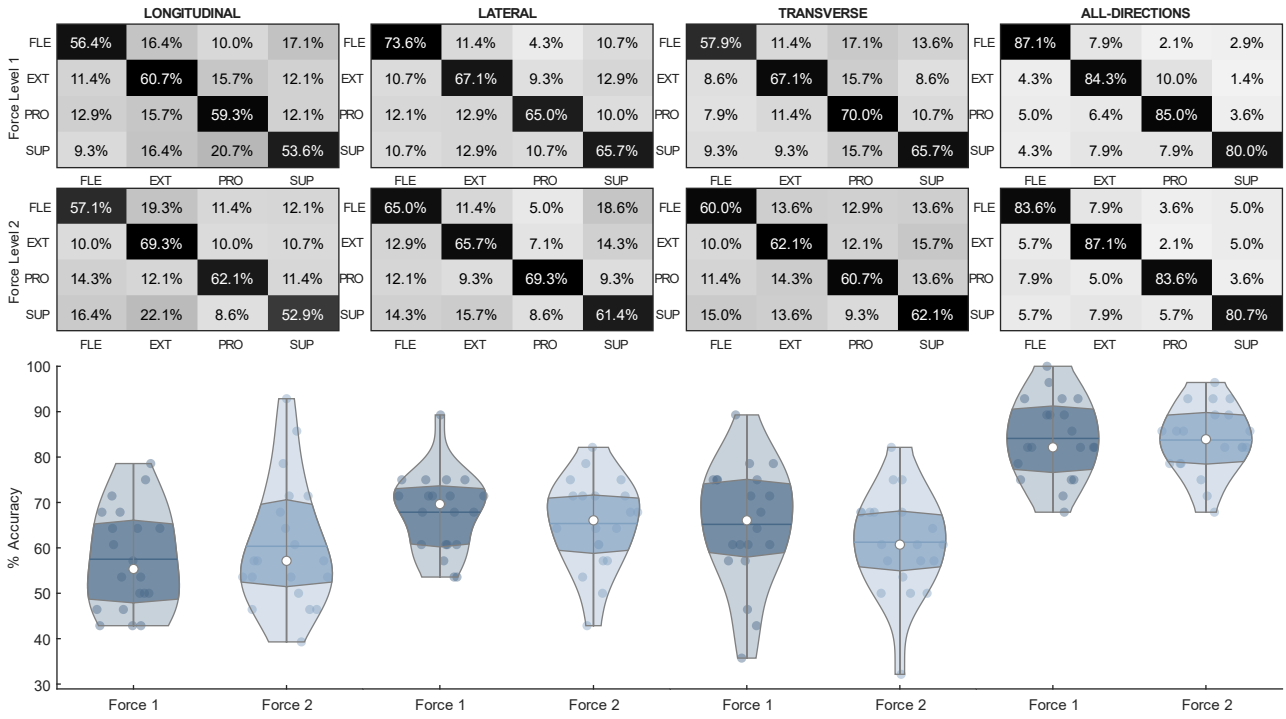

Figure 7. Top. Confusion matrices of classification accuracy of gestures for models based on every single axis and the combination of axes (last column) of vMMG for each level of contact force. Bottom. Violin plots illustrate the distribution of the classification accuracies of the models across participants for single- and multi-axis-based models for each level of contact force.

Table 1. Statistical Comparison for Classification Performance

Force Level	Direction	∗	Probability
FL1 vs FL2	Longitudinal		p: 0.253
	Lateral		p: 0.383
	Transverse		p: 0.235
	All-Directions		p: 0.884
FL1	Longitudinal vs. All	∗	p: 4.162e-10
	Lateral vs. All	∗	p: 2.672e-07
	Transverse vs. All	∗	p: 6.799e-09
FL2	Longitudinal vs. All	∗	p: 8.451e-09
	Lateral vs. All	∗	p: 7.214e-07
	Transverse vs. All	∗	p: 5.277e-08

Statistical comparison between uni-directional and . multi-directional trained classification models. Significance is marked ∗ and shown in red color for the Bonferroni-adjusted value of *adjusted-p-value*<0.0166, df=3

3.5. Statistical Analysis

There is a lack of investigations in the analysis of the effect on the MMG signal quality when using different levels of contact force. In this study, results of the different levels of contact force on VMMG show that both temporal and spectral features of the signal are affected in a multi-directional manner and these changes are captured along the different directions of vMMG. However, statistical comparison between forces for the spectrotemporal feature changes showed no significant differences ($p > 0.05$) of features between the first and the second level of contact force. The non-parametric Wilcoxon signed rank test showed significant differences at ($p < 0.05$) between levels of force for GE and CC for the second and the third frequency components for Extension and Pronation. However, these differences were not significant at the adjusted p-value ($p > 0.0041$). No other significant differences were found between the first and second levels of contact force for global efficiency and clustering coefficient along any of the directions of MMG propagation. In terms of classification of gestures, accuracies were statistically compared between levels of force for each direction and the combination of directions. No significant differences ($p > 0.05$) were found between the classification performance of force level one and force level two for all trained models. Statistical comparison between classification models trained using features from each individual direction vs the multi-directional trained model show statistical significance ($p < 0.0166$) for all models for both levels of contact force. Table 1 summarizes the statistical results of the comparison between levels of force and between classification models. Significant differences between gestures are shown in red.

This study is motivated by findings in the literature demonstrating the relevance of MMG for the analysis of neurophysiological parameters involved during motor function [62,63], by the recent studies in muscle connectivity networks [15,50] and by the recent investigation on the application of MMG for muscle connectivity analysis [21]. The present results show further evidence that mechanomyography can be used as a tool for functional muscle connectivity analysis. Muscle connectivity results show distinct topologies depending on frequency, gesture, and direction. The differences in connectivity strength between muscles for the multiple gestures suggest a characteristic spectral profile at the different frequency ranges driven by muscle activity during gestures. The analysis of muscle connectivity as shown in Figure 4 shows a clear distinction of functional activity of muscles based on the gesture, which can be registered by MMG. This study also shows for the first time the use of intermuscular coherence derived from MMG for the classification of motor tasks. As shown, the use of IMC obtained from each individual direction yields a relatively high classification accuracy which can be enhanced by the combination of IMC across directions, providing a more robust framework for the classification of gestures. Furthermore, this study also provides additional evidence of spectrotemporal feature variations based on the level of contact force between the sensor and the skin for vMMG. Results show that the temporal and spectral space of vMMG varies minimally when increasing the level of contact force. It is worth mentioning that the design of the sensor allows for the increase in contact pressure on the muscle while adding no extra weight to the sensor, which could explain the different findings reported in [29].

4. Conclusion

In this study we introduced: a) the analysis of intermuscular coherence based on vMMG extracted from four superficial muscles around the forearm, b) the analysis of multi-dimensional muscle networks derived from the different directions of propagation with respect to the muscle fiber alignment, c) the use of IMC for the generation of classification models for the identification of multiple hand gesture tasks, and d) the analysis of vMMG network information in terms of quality and discriminative power when different sensor-skin contact force levels are applied. The results show distinct topologies of multi-directional muscle networks across frequency components, gestures, and directions. The analysis of vMMG properties for the generation of muscle connectivity networks showed no significant changes in classification accuracy between contact force levels. Results of the classification accuracy between uni-directional and multi-directional trained models showed significant differences between all uni-directional trained models when compared to the model trained using the combination of all directions for both levels of contact force. The findings of this investigation support the usability of vMMG as a tool for functional muscle connectivity analysis and provide evidence of the unique spectral characteristics of the vMMG signal detected along the different directions of propagation when performing various motor tasks, enabling the applicability of classification models based on IMC. In addition, the present results show evidence that the network properties of vMMG do not vary significantly when a higher level of contact force is applied. Lastly, as a future perspective of this work, the results presented in this study motivate the investigation of muscle network analysis based on vMMG during complex dynamic motor tasks involving a higher number of muscles and the use of more sophisticated algorithms for motor activity detection of a higher number of dynamic and static tasks.

Acknowledgments

This work was supported in part by the UK EPSRC EP/W524323, UK Dementia Research Institute Care-Research Technology Centre (DRI-CRT), Imperial College Department of Mechanical Engineering, and US National Science Foundation (Awards 2037878; 2031594).

References

[1] C. M. Gray and W. Singer. Stimulus-specific neuronal oscillations in orientation columns of cat visual cortex. *Proceedings of the National Academy of Sciences*, 86(5):1698–1702, 1989.

[2] S. Mehrkanoon et al. Low-dimensional dynamics of resting-state cortical activity. *Brain topography*, 27(3):338–352, 2014.

[3] J. I. Chapeton et al. Large-scale communication in the human brain is rhythmically modulated through alpha coherence. *Current Biology*, 29(17):2801–2811.e5, 2019.

[4] B. C. van Wijk et al. Neural synchrony within the motor system: what have we learned so far? *Frontiers in human neuroscience*, 6:252, 2012.

[5] K. Nazarpour et al. Flexible cortical control of task-specific muscle synergies. *Journal of Neuroscience*, 32(36):12349–12360, 2012.

[6] I. E. de Vries et al. Functional connectivity in the neuromuscular system underlying bimanual coordination. *Journal of neurophysiology*, 116(6):2576–2585, 2016.

[7] E. Bizzi and V. C. Cheung. The neural origin of muscle synergies. *Frontiers in Computational Neuroscience*, 7:51, 2013.

[8] J. H. McAuley and C. D. Marsden. Physiological and pathological tremors and rhythmic central motor control. *Brain*, 123(8):1545–1567, 08 2000.

[9] T. W. Boonstra et al. Muscle networks: Connectivity

analysis of emg activity during postural control. *Scientific Reports*, 5(1):17830, Dec 2015.

[10] E. Bullmore and O. Sporns. Complex brain networks: graph theoretical analysis of structural and functional systems. *Nature reviews neuroscience*, 10(3):186–198, 2009.

[11] M. Rubinov and O. Sporns. Complex network measures of brain connectivity: Uses and interpretations. *NeuroImage*, 52(3):1059–1069, 2010. Computational Models of the Brain.

[12] C. M. Laine and F. J. Valero-Cuevas. Intermuscular coherence reflects functional coordination. *Journal of neurophysiology*, 118(3):1775–1783, Sep 2017.

[13] J. N. Kerkman et al. Functional connectivity analysis of multiplex muscle network across frequencies. In *2017 39th Annual International Conference of the IEEE Engineering in Medicine and Biology Society (EMBC)*, pp. 1567–1570, 2017.

[14] J. N. Kerkman et al. Network structure of the human musculoskeletal system shapes neural interactions on multiple time scales. *Science Advances*, 4(6), 2018.

[15] J. N. Kerkman et al. Muscle synergies and coherence networks reflect different modes of coordination during walking. *Frontiers in Physiology*, 11:751, 2020.

[16] T. W. Boonstra and M. Breakspear. Neural mechanisms of intermuscular coherence: implications for the rectification of surface electromyography. *Journal of Neurophysiology*, 107(3):796–807, 2012. PMID: 22072508.

[17] A. Phinyomark et al. Surface electromyography (emg) signal processing, classification, and practical considerations. *Biomedical Signal Processing: Advances in Theory, Algorithms and Applications*, pp. 3–29, 2020.

[18] H. R. Marateb et al. Reliable and accurate information extraction from surface electromyographic signals. In *Modelling and Analysis of Active Biopotential Signals in Healthcare, Volume 1*. IOP Publishing, 2020.

[19] M. O. Ibitoye et al. Mechanomyography and muscle function assessment: A review of current state and prospects. *Clinical Biomechanics*, 29(6):691–704, 2014.

[20] R. B. Woodward et al. Pervasive monitoring of motion and muscle activation: Inertial and mechanomyography fusion. *IEEE/ASME Transactions on Mechatronics*, 22(5):2022–2033, 2017.

[21] C. S. M. Castillo et al. Synergistic upper-limb functional muscle connectivity using acoustic mechanomyography. *IEEE Transactions on Biomedical Engineering*, 2022.

[22] J. V. Frangioni et al. The mechanism of low-frequency sound production in muscle. *Biophysical journal*, 51(5):775–783, 1987.

[23] G. Gordon and A. Holbourn. The sounds from single motor units in a contracting muscle. *The Journal of physiology*, 107(4):456, 1948.

[24] A. Jaskólska et al. The effect of skinfold on frequency of human muscle mechanomyogram. *Journal of Electromyography and Kinesiology*, 14(2):217–225, 2004.

[25] C. Cescon et al. Longitudinal and transverse propagation of surface mechanomyographic waves generated by single motor unit activity. *Medical & Biological Engineering & Computing*, 46(9):871–877, 2008.

[26] A. Archer et al. Propagation direction of natural mechanical oscillations in the biceps brachii muscle during voluntary contraction. *Journal of electromyography and kinesiology : official journal of the International Society of Electrophysiological Kinesiology*, 22:51–9, 11 2011.

[27] M. Stokes and P. Dalton. Acoustic myographic activity increases linearly up to maximal voluntary isometric force in the human quadriceps muscle. *Journal of the neurological sciences*, 101(2):163–167, 1991.

[28] C. F. Bolton et al. Recording sound from human skeletal muscle: technical and physiological aspects. *Muscle & Nerve: Official Journal of the American Association of Electrodiagnostic Medicine*, 12(2):126–134, 1989.

[29] M. Watakabe et al. Reliability of the mechanomyogram detected with an accelerometer during voluntary contractions. *Medical and Biological Engineering and Computing*, 41(2):198–202, 2003.

[30] I. Talib et al. Association of anthropometric parameters with amplitude and crosstalk of mechanomyographic signals during forearm flexion, pronation and supination torque tasks. *Scientific reports*, 9(1):1–12, 2019.

[31] C. S. M. Castillo et al. Wearable mmg-plus-one armband: Evaluation of normal force on mechanomyography (mmg) to enhance human-machine interfacing. *IEEE Transactions on Neural Systems and Rehabilitation Engineering*, 29:196–205, 2021.

[32] E. Krueger et al. Advances and perspectives of mechanomyography. *Revista Brasileira de Engenharia Biomédica*, 30(4):384–401, 2014.

[33] Y. Itoh et al. Spectrum analysis of the mechanomyogram: elimination of the longitudinal shortening component of muscle fibers. *Systems and Computers in Japan*, 31(13):57–64, 2000.

[34] W. Youn and J. Kim. Feasibility of using an artificial neural network model to estimate the elbow flexion force from mechanomyography. *Journal of neuroscience methods*, 194(2):386–393, 2011.

[35] C. Orizio et al. Spectral analysis of muscular sound during isometric contraction of biceps brachii. *Journal of Applied Physiology*, 68(2):508–512, 1990. PMID: 2318762.

[36] A. Bruns. Fourier-, hilbert- and wavelet-based signal analysis: are they really different approaches? *Journal of Neuroscience Methods*, 137(2):321–332, 2004.

[37] P. Bloomfield. *Fourier analysis of time series: an introduction*. John Wiley & Sons, 2004.

[38] A. S. Wee and R. A. Ashley. Vibrations and sounds produced during sustained voluntary muscle contraction. *Electromyography and clinical neurophysiology*, 29 6:333–7, 1989.

[39] J. H. McAuley et al. Frequency peaks of tremor, muscle vibration and electromyographic activity at 10 hz, 20 hz and 40 hz during human finger muscle contraction may reflect rhythmicities of central neural firing. *Experimental Brain Research*, 114(3):525–541, May 1997.

[40] C. Orizio et al. Muscular sound and force relationship during isometric contraction in man. *European Journal of Applied Physiology and Occupational Physiology*, 58(5):528–533, 1989.

[41] I. Talib et al. A systematic review of muscle activity assessment of the biceps brachii muscle using mechanomyography. *Journal of musculoskeletal & neuronal interactions*, 18(4):446, 2018.

[42] D. C. Toledo-Pérez et al. Support vector machine-based emg signal classification techniques: A review. *Applied Sciences*, 9(20):4402, 2019.

[43] K. Akataki et al. Age-related change in motor unit activation strategy in force production: a mechanomyographic investigation. *Muscle & nerve*, 25(4):505–512, 2002.

[44] T. W. Beck et al. Mechanomyographic amplitude and mean power frequency versus torque relationships during isokinetic and isometric muscle actions of the biceps brachii. *Journal of Electromyography and Kinesiology*, 14(5):555–564, 2004.

[45] R. Uwamahoro et al. Assessment of muscle activity using electrical stimulation and mechanomyography: a systematic review. *Biomedical engineering online*, 20(1):1–47, 2021.

[46] N. Alves and T. Chau. Uncovering patterns of forearm

muscle activity using multi-channel mechanomyography. *Journal of electromyography and kinesiology*, 20(5):777–786, 2010.

[47] D. Tkach et al. Study of stability of time-domain features for electromyographic pattern recognition. *Journal of neuroengineering and rehabilitation*, 7(1):1–13, 2010.

[48] J. Xie et al. Estimation of triceps muscle strength based on mechanomyography. In *Journal of Physics: Conference Series*, volume 1544, pp. 012055. IOP Publishing, 2020.

[49] K. Terry and L. Griffin. How computational technique and spike train properties affect coherence detection. *Journal of Neuroscience Methods*, 168(1):212–223, 2008.

[50] M. Houston et al. Alterations in muscle networks in the upper extremity of chronic stroke survivors. *IEEE Transactions on Neural Systems and Rehabilitation Engineering*, 29:1026–1034, 2021.

[51] D. Farina et al. Motor unit acceleration maps and interference mechanomyographic distribution. *Journal of biomechanics*, 41:2843–9, 09 2008.

[52] C. Orizio et al. Transients of the force and surface mechanomyogram during cat gastrocnemius tetanic stimulation. *European journal of applied physiology*, 88(6):601–606, 2003.

[53] M. Ouamer et al. Acoustic myography during voluntary isometric contraction reveals non-propagative lateral vibration. *Journal of Biomechanics*, 32(12):1279–1285, 1999.

[54] C. Orizio et al. The surface mechanomyogram as a tool to describe the influence of fatigue on biceps brachii motor unit activation strategy. historical basis and novel evidence. *European Journal of Applied Physiology*, 90(3):326–336, Oct 2003.

[55] M. A. Islam et al. Mechanomyography sensor development, related signal processing, and applications: A systematic review. *IEEE Sensors Journal*, 13:2499–2516, 2013.

[56] I. Talib et al. Choice of mechanomyography sensors for diverse types of muscle activities. *Journal of Telecommunication, Electronic and Computer Engineering*, 10:79–82, 2018.

[57] F. Esposito et al. Electromechanical delays during a fatiguing exercise and recovery in patients with myotonic dystrophy type 1. *European journal of applied physiology*, 117:551–566, 2017.

[58] P. Kaczmarek et al. Towards sensor position-invariant hand gesture recognition using a mechanomyographic interface. In *2017 Signal Processing: Algorithms, Architectures, Arrangements, and Applications (SPA)*, pp. 53–58, 2017.

[59] W. Guo et al. Mechanomyography assisted myoeletric sensing for upper-extremity prostheses: A hybrid approach. *IEEE Sensors Journal*, 17(10):3100–3108, 2017.

[60] M. M. Ismail et al. Hand motion pattern recognition analysis of forearm muscle using mmg signals. *Bulletin of Electrical Engineering and Informatics*, 8(2):533–540, 2019.

[61] Y. Rajamani et al. Analysis and classification of multiple hand gestures using mmg signals. *Journal of Telecommunication, Electronic and Computer Engineering (JTEC)*, 10(1-13):67–71, 2018.

[62] E. D. Ryan et al. Time and frequency domain responses of the mechanomyogram and electromyogram during isometric ramp contractions: A comparison of the short-time fourier and continuous wavelet transforms. *Journal of Electromyography and Kinesiology*, 18(1):54–67, 2008.

[63] T. W. Beck et al. Does the frequency content of the surface mechanomyographic signal reflect motor unit firing rates? a brief review. *Journal of Electromyography and Kinesiology*, 17(1):1–13, 2007.